

# Error Analysis of the OTDOA From the Resolved First Arrival Path in LTE

Seung-Hyun Kong, *Senior Member, IEEE*, and Binhee Kim, *Member, IEEE*

**Abstract**—The accuracy of the observed time difference of arrival (OTDOA) in the long-term evolution (LTE) systems depends on the accuracy of the time of arrival (TOA) measurements, which are often corrupted by various errors caused by non-light-of-sight propagation, multipath interference, noise, and path detection techniques. Furthermore, signal bandwidth, channel condition, distance from the evolved node-B, and scatterer distribution are the affecting parameters on the OTDOA accuracy. Since the user equipment obtains the most accurate TOA from the resolved first arrival path (R-FAP), understanding errors of the TOA and OTDOA from the R-FAP is necessary to develop OTDOA positioning techniques. In this paper, we develop theoretical expressions for the TOA and OTDOA error distributions of the R-FAP for outdoor multipath environments by integrating theoretical models of the errors expressed with the affecting parameters, and theoretical expressions are verified with numerous Monte Carlo simulations. In addition, we propose an LTE OTDOA positioning technique that compensates the mean TOA offset in the TDOA measurements before applying a positioning algorithm, and we demonstrate the performance improvement using Monte Carlo simulations. In this paper, we do not include OTDOA errors due to the network synchronization and intercell interference.

**Index Terms**—OTDOA, LTE, multipath, first arrival path.

## I. INTRODUCTION

SINCE U.S. federal communication commission (FCC) issued the emergency 911 (E911) mandate, in 1996, that requires accurate location estimate of mobile emergency callers [1], a number of mobile positioning techniques have been developed and used in wireless communication systems. Among the techniques, assisted global positioning systems (A-GPS) [2] has been the most widely used technology and the key enabler of location based services (LBS). However, the accuracy and availability of GPS are severely degraded in many urban and indoor environments, so there has been a strong demand for user equipment (UE) positioning based on non-GPS signals.

In the long-term evolution (LTE) systems, the observed time difference of arrival (OTDOA) positioning technique is one

Manuscript received July 22, 2015; revised December 19, 2015 and April 8, 2016; accepted June 20, 2016. Date of publication June 29, 2016; date of current version October 7, 2016. This work (2013R1A2A2A01067863) was supported by Mid-career Researcher Program through NRF grant funded by the Korean government (MEST). The associate editor coordinating the review of this paper and approving it for publication was A. Giorgetti.

The authors are with the CCS Graduate School for Green Transportation, Korea Advanced Institute of Science and Technology, Daejeon 305-701, South Korea (e-mail: skong@kaist.ac.kr; vini@kaist.ac.kr).

Color versions of one or more of the figures in this paper are available online at <http://ieeexplore.ieee.org>.

Digital Object Identifier 10.1109/TWC.2016.2586469

of the major UE positioning techniques that can provide a position fix in any environments. For OTDOA positioning [3], UE detects the time of arrival (TOA) of the first arrival path among the resolved paths for all downlinks of associated evolved node-Bs (ENBs) and obtains OTDOA measurements. Besides OTDOA, TOA is the essential measurement for other radio-location techniques such as GPS, advanced forward link trilateration (AFLT) [4], and enhanced observed time difference (E-OTD) [5]. However, it has been found that TOA measurement accuracy is easily degraded by multiple errors, and that it is difficult for a TDOA (OTDOA) positioning technique to improve positioning accuracy beyond the E911 mandate in urban and indoor environments [6]. Therefore, investigating the TOA errors is one of the most fundamental issues in the study of TDOA (OTDOA) positioning techniques.

In practice, there are multiple causes for TOA measurement errors; small probability of line-of-sight (LOS) path detection  $P_{\text{LOS}}$  as shown in Table 7.2.-2 of [7] means that LOS path may be not observable and a TOA measurement obtained from later arriving multipath introduces an inevitable excess delay. In practice, a number of strong multipath constructs a different (usually smaller) number of resolvable (or resolved) paths, so UEs, utilizing signal processing techniques, needs to measure TOA from the resolved first arrival path (R-FAP) among the resolved paths. Therefore, the TOA measurements are often corrupted by the multipath interference (MI), accuracy of the employed signal processing techniques, and noise in the received signal. Note that the measured TOA from the R-FAP is potentially different from the TOA of the true FAP (T-FAP), that is, the true first arriving individual path. In addition, signal bandwidth, channel condition, distance from ENB, elevation angle, and scatterer distribution (i.e., environments) are affecting factors on the measured TOA accuracy.

In [8], closed-form expressions for TOA and angle of departure (AOD) distributions of the T-FAP are found for downlink Gaussian Scatterer Distribution Model (GSDM) and USDM (Uniform SDM); however, the expressions in [8] do not include TOA errors due to the MI, TOA detection function, and noise. In [9], expression for the TOA error PDF of the R-FAP in GPS is found for an exponential scatterer distribution that is a function of the satellite elevation angle, which agrees with field observations [10]. However, GPS elevation angle is generally much higher than LTE downlinks, and GPS TOA error PDF has a very narrow distribution with maximum of a half chip delay [10] resulting in only one resolved path [9]

in practice, whereas LTE downlinks have multiple resolved paths very often. In addition, GPS TOA detection functions are based on narrow correlators [11], while UE utilizes a matched filter based path detection technique [12] or enhanced path resolution techniques [13]–[15].

Despite the significant effects on OTDOA-based positioning accuracy, the TOA error of the R-FAP in LTE has been little studied. In [16], fundamental limits in the ranging accuracy of orthogonal frequency division multiplexing (OFDM) signals are studied for multipath channels, but it does not provide error distributions of the measured delays of OFDM signals by receivers. In the literature, Extended pedestrian A model (EPA), extended vehicular A model (EVA), extended typical urban model (ETU) [17], and WINNER model [18] have been used to evaluate TDOA positioning techniques in LTE. However, even though EPA, EVA, and ETU may produce time-varying TOA measurements due to the independent fading of tap components constituting the R-FAP, those models are based on fixed tap-delays, where the relative delay of the T-FAP (first tap component) is fixed [17]. The WINNER model [18] provides a statistical TOA distribution, where the T-FAP does not have a fixed delay, but the model does not deliver any insights into the contribution of the various error components. In [19] and [20], TDOA positioning error is discussed, but the theoretical analysis to investigate the TDOA error is not introduced sufficiently. In [21] and [22], on the other hand, TDOA error distributions are obtained empirically for an indoor area and an outdoor-to-indoor scenarios, but the studies do not introduce theoretical analysis of the distributions.

Since LTE network synchronization error can be eliminated using GPS embedded in ENB or using Precision Time Protocol (PTP) [23], investigating OTDOA error is equivalent to understanding the TDOA error. In this paper, we investigate the TOA and TDOA errors in the measurements of LTE positioning reference signal (PRS) for outdoor multipath environments, and based on the downlink GSMD we develop theoretical expressions of the TOA and TDOA error distributions of the R-FAP for Rician and Rayleigh channels. The theoretical expressions derived in this paper integrate theoretical error models for TOA detection function, multipath delay distribution, multipath interference (MI), and noise, which are expressed in terms of the number of resource blocks (RB), channel condition, downlink distance, and scatterer distribution. Based on the TOA and TDOA error distribution models, we propose a TDOA offset compensation technique that can improve TDOA positioning accuracy.

This paper is organized as follows. Section II finds expressions for overall TOA and TDOA error distributions, and Section III-A derives expressions for the probability density function (PDF) and cumulative density function (CDF) of TOA errors of small excess delays, MI error PDF for Rician and Rayleigh channels, and noise error PDF. By integrating the error components, closed-form expressions for the complete TOA and TDOA error PDF of the R-FAP are derived in Section III-B and Section IV, respectively. We propose a TDOA performance improvement technique, and the derived

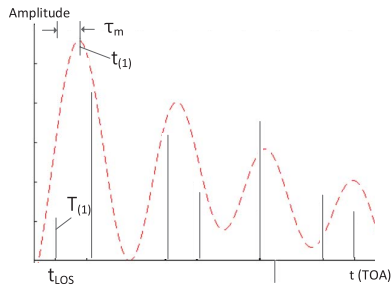


Fig. 1. TOA error of resolved first arrival path in an ACF output.

TOA and TDOA error models are compared to the TOA and TDOA error histograms found with numerous Monte Carlo simulations for various signal conditions in Section V. It is demonstrated that the proposed TDOA positioning technique can improve TDOA positioning performance in multipath environments. Finally, Section VI draws the conclusion of the paper.

## II. TOA ERROR COMPONENTS IN LTE

When ENB antenna is above the surrounding objects and buildings, downlink scatterer distribution can be approximated by the Gaussian scatterer distribution model (GSMD) [8], [24], where the scatterers are in a circular scattering region around UE, and the scatter density decreases with the distance from the UE [25].

In LTE systems, the shape of ACF output envelope for a single path is similar to a sinc function (discussed in Section III-B) so that the true first arrival individual path (T-FAP) and multipath arriving no later than the maximum correlation lag, that is inversely proportional to the bandwidth of the LTE PRS [26], from the T-FAP can construct just one resolved path. In other words, the discrete auto-correlation function (ACF) output looks like from a single path. Let the T-FAP have a TOA  $T_{(1)}$  and  $t_{(1)}$  be the measured TOA of the resolved path using a matched filter based TOA detection function [12], [21], and [27]. Note that, in general,  $t_{(1)} \neq T_{(1)}$  due to the multipath interference (MI) by the closely arriving multipath.

In rich multipath environments such as dense urban and urban area, there are often multiple resolved paths observed in the discrete ACF output, as illustrated with an example for a noiseless case in Fig. 1. As shown, there are  $M$  ( $= 8$ ) individual multipath arriving at the UE; their amplitudes and delays are illustrated with solid lines along the TOA axis, and the continuous-time envelope of the resulting ACF output is in a dashed line. From the envelop, UE may be able to resolve  $m$  ( $= 4 < M$ ) paths, since there are groups of multipath arriving closely. Note that the base span of the mainlobe of an ACF output depends on the number of resource blocks (RBs) for positioning reference signal (PRS). The number of RBs can be flexible, and therefore, the base span can be much narrower than the example in Fig. 1, in which case  $m > 4$  may be observed. Note also that we neglect the effect of the sidelobes of the ACF output in the example. Among the  $m$  resolved paths, UE detects the TOA of the first resolved

path (or resolved first arrival path, R-FAP) and returns  $t_{(1)}$  as the most accurate TOA measurement. In Fig. 1, when the attenuated T-FAP has a TOA of the LOS path  $t_{\text{LOS}}$ , and the MI error is defined as

$$\tau_m = t_{(1)} - T_{(1)}. \quad (1)$$

As depicted in Fig. 1, the MI error depends not only on the relative amplitude (including phase) and delay, but also on the employed TOA detection function, since the function produces the measurement  $t_{(1)}$ . Note that when the LOS path is completely blocked and faded, the T-FAP is not the LOS path and has a NLOS propagation, in which case it is expected that  $T_{(1)}$  is larger than the TOA of the LOS path  $t_{\text{LOS}} = D/c$ , where  $D$  is the downlink distance (i.e., distance between UE and ENB) and  $c$  is the speed of light. In other words, for NLOS channel,

$$\tau_e = T_{(1)} - \tau_{\text{LOS}}, \quad (2)$$

is the excess delay of the T-FAP due to the NLOS propagation. However, in this paper, we assume that the LOS path may severely attenuated but not completely lost so that the T-FAP is the LOS path and  $\tau_e$  is negligible.

In [8], it is found that the TOA distribution of the T-FAP can be expressed using the first order statistics [28] as

$$f_{T_{(1)},2}(t) = M[1 - F_t(t)]^{M-1} f_t(t), \quad (3)$$

where  $F_t(t)$  and  $f_t(t)$  are the TOA error CDF and TOA error PDF for a received path, respectively,  $(\cdot)_2$  represents the Rayleigh channel, and  $M$  is the number of all (individual) multipath arriving at UE. In a viewpoint, (3) expresses the fact that given the  $f_t(t)$  a larger number of later arrival paths enhances the confidence that the T-FAP is closer to the TOA of the LOS. Note that in Rician channel T-FAP is always the LOS path so that

$$f_{T_{(1)},1}(t) = \delta(t - D/c), \quad (4)$$

where  $(\cdot)_1$  is for the Rician channel.

When only  $m (< M)$  paths are resolved, the UE should measure the TOA of the R-FAP, i.e.,  $t_{(1)}$  [12]. In practice, noise  $n(t)$  introduces additional TOA error  $\tau_n$  that can be approximated by a Gaussian distribution  $\mathcal{N}(0, \sigma_n^2)$  [27]. Since the noise is independent of the TOA of the R-FAP, the measured TOA error PDF of the R-FAP in noisy channel is expressed as

$$f_{t_{(1)}}(t) = f_{T_{(1)}}(t) * f_{\tau_m}(t) * f_{\tau_n}(t) \quad (5)$$

where ‘\*’ is the convolution operator, and  $f_{\tau_m}(t)$  and  $f_{\tau_n}(t)$  represent the MI error PDF (i.e., TOA error PDF due to the MI) and the noise error PDF, respectively. Note that while  $M$  and  $f_{T_{(1)}}(t)$  depend on the downlink scatterer distribution and environments,  $f_{\tau_m}(t)$  depends on both the multipath delay distribution and the performance of the TOA detection function, and  $f_n(t)$  depends on the signal-to-noise ratio (SNR). Note also that  $f_{T_{(1)}}(t)$  in (5) can be  $f_{T_{(1)},1}(t)$  for Rician channels or  $f_{T_{(1)},2}(t)$  for Rayleigh channels depending on the

channel condition. As a result, the TDOA error PDF can be expressed as

$$f_{dt_{(1)}}^{(i,j)}(t) = f_{t_{(1)}}^{(i)}(t) * f_{t_{(1)}}^{(j)}(-t), \quad (6)$$

where  $d(\cdot)$  represents the difference of the quantity  $(\cdot)$ ,  $(\cdot)^{(i,j)}$  represents the TDOA between ENB $_i$  and ENB $_j$ , and  $(\cdot)^{(i)}$  and  $(\cdot)^{(j)}$  are for the PRS signals from ENB $_i$  and ENB $_j$ , respectively.

In the following sections, we derive an approximate theoretical expressions for  $f_t(t)$  and  $f_{\tau_m}(t)$  for LTE PRS signals in Rician and Rayleigh channels to find closed-form expressions for TOA error PDF  $f_{t_{(1)}}(t)$  and TDOA error PDF  $f_{dt_{(1)}}(t)$ .

### III. TOA, MI, AND NOISE ERROR PDFS

In this section, we derive simplified mathematical expressions for the TOA error PDF based on GSDM and the MI error PDF for Rayleigh and Rician channels. To derive the PDFs, we utilize three assumptions to simplify the algebraic expressions and derivations. The first assumption is that the excess delay  $\tau$  considered in the derivation of the TOA error PDF is very small. This assumption is valid, since  $f_{t_{(1)}}(t)$  has most of the density at very small excess delays, i.e.,  $t - D/c$ , for large  $M$  representing rich multipath environments. The second assumption is that the R-FAP is stronger than the other later resolved paths. This is valid in a statistical view, since the power delay spectrum (PDS) is a monotonously decreasing function with respect to the excess delay [24]. The third assumption is that the T-FAP and multipath constituting the R-FAP can be divided into two dominant groups of paths with similar excess delays [9]. The third assumption may be not representative for all cases in practice but provides a useful way to analyze and to model the MI errors.

#### A. Approximate GSDM-Based TOA Error PDF

A complete mathematical expression for  $f_t(t)$ , the TOA error PDF of a downlink multipath for GSDM is available from [8] and shown in the Appendix section. Assuming very small excess delays  $t - D/c$ , we can develop a simplified algebraic expression for the TOA error PDF.

In the following, we exploit the approximation [29]

$$\begin{aligned} Q(x) &= \frac{1}{\sqrt{2\pi}} \int_x^\infty e^{-\frac{t^2}{2}} dt \\ &\simeq \frac{1}{2\sqrt{2\pi} \cdot \sqrt{1+x^2/2}} \exp\left(-\frac{x^2}{4}\right) \\ &\simeq \frac{1}{2\sqrt{2\pi}} \exp\left(-\frac{x^2}{4}\right) \end{aligned} \quad (7)$$

for a small  $x$ , and since  $tc - D$  is a small positive value,  $\phi_0$  [8] is negligibly small for small TOA  $t$ , and

$$r_1 \approx tc - D = 2r_0 \rightarrow 0, \quad (8)$$

where  $r_1$  and  $r_0$  are the distance  $r$  for  $\phi = \pi$  and  $\phi = \pi/2$ , respectively. Utilizing  $\phi_0 \approx 0$  and (8), the TOA error PDF

$f_t(t)$  in [8] can be simplified to

$$\begin{aligned} f_t(t) &\simeq \frac{c}{\pi D} \left[ \exp\left(-\frac{r_1^2}{2\sigma^2}\right) - \exp\left(-\frac{r_0^2}{2\sigma^2}\right) \right] \\ &+ \frac{(\pi-2)r_0c}{4\pi\sigma^2} \exp\left(-\frac{r_0^2}{2\sigma^2}\right) \\ &+ \frac{1}{\pi} \exp\left(-\frac{r_1^2}{2\sigma^2}\right) \left( \phi'_0 - \frac{c\pi}{2R} \right) + \frac{c}{\pi\sigma^2} \exp\left(-\frac{r_1^2}{2\sigma^2}\right) \\ &\times \left[ 2r_0\left(\frac{\pi}{2} - \phi_0 - 1 + \frac{\pi r_1}{2R}\right) + 2r_0 - \frac{\pi r_1}{2} \right] \\ &+ \frac{1}{2\sigma\pi} \left[ c \exp\left(-\frac{r_0^2}{4\sigma^2}\right) + \left(\frac{c\pi}{2} - c\right) \exp\left(-\frac{r_1^2}{4\sigma^2}\right) \right] \quad (9) \end{aligned}$$

for  $t > D/c$ , where

$$\begin{aligned} r_1 &\simeq \frac{tc - D}{2} \\ \phi'_0 &\simeq \frac{tc^2}{RD} - \frac{c}{D} \simeq c\left(\frac{1}{R} - \frac{1}{D}\right). \end{aligned}$$

Therefore, (9) can be rearranged to

$$\begin{aligned} f_t(t) &\approx \frac{c}{\pi} \left[ \frac{(1-\pi/2)}{R} - \frac{\pi(tc-D)}{2\sigma^2} \right] \exp\left(-\frac{r_1^2}{2\sigma^2}\right) \\ &+ \frac{c}{\pi} \left[ \frac{(\pi-2)(tc-D)}{8\sigma^2} - \frac{1}{D} \right] \exp\left(-\frac{r_0^2}{2\sigma^2}\right) \\ &+ \frac{c}{2\pi\sigma} \exp\left(-\frac{r_0^2}{4\sigma^2}\right) \\ &+ \frac{c^2}{2\pi\sigma} \left(\frac{\pi}{2} - 1\right) \exp\left(-\frac{r_1^2}{4\sigma^2}\right). \quad (10) \end{aligned}$$

Since  $\tau$  denotes the excess delay of multipath as

$$\tau = t - \frac{D}{c}, \quad (11)$$

any expression in TOA  $t$  in this paper can be directly expressed in terms of the excess delay  $\tau$ . Therefore, (10) can be expressed as

$$\begin{aligned} f_\tau(\tau) &\approx K_G \exp\left(-\frac{r_0^2}{4\sigma^2}\right) \Big|_{t=\tau+D/c} \\ &\approx \frac{1}{2\sigma_c\pi} \exp\left(-\frac{\tau^2}{16\sigma_c^2}\right) \quad (12) \end{aligned}$$

for small  $\tau > 0$ , where  $\sigma_c = \sigma/c$ , and  $K_G$  is a normalization constant. From (12), the CDF for small  $\tau$  is found using (7) as

$$\begin{aligned} F_\tau(\tau) &= 1 - 2Q\left(\frac{\tau}{2\sqrt{2}\sigma_c}\right) \\ &\approx 1 - \frac{1}{\sqrt{2}\pi} \exp\left(-\frac{\tau^2}{32\sigma_c^2}\right). \quad (13) \end{aligned}$$

Note that  $\sigma_c$  represents the spread of scatterers of downlink, which is found to be proportional to the downlink distance  $D$  in urban environments [25], [30], for example, empirical data shows that  $\sigma \simeq 0.337D$  for urban environments and  $\sigma \simeq 0.113D$  for rural environments.

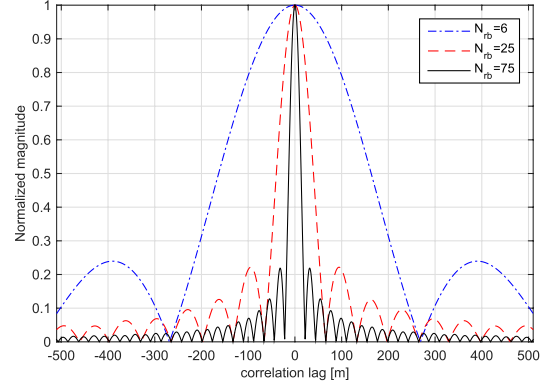


Fig. 2. Examples of LTE PRS ACF for some  $N_{rb}$ .

### B. MI Error PDF

The MI error  $\tau_m$  occurs when the ACF output of T-FAP is distorted by the following closely-arriving multipath, and the MI error depends on the shape and size of the ACF output of the LTE PRS, as discussed in Section II.

It is found that the ACF output of a single path LTE PRS for a subcarrier spacing  $\Delta f_{sc} = 15\text{kHz}$  is obtained based on the normalized ACF output derived in [26] as

$$\begin{aligned} R_L(\tau) &= \frac{2P}{N_{rs}^2} \times \cos\left(\frac{(6N_{rb}+1)\pi\tau}{N_{rs}}\right) \times \frac{\sin\left(\frac{6\pi N_{rb}\tau}{N_{rs}}\right)}{\sin\left(\frac{6\pi\tau}{N_{rs}}\right)} \\ &\times \exp\left(\frac{j(5+2\theta_{rs})\pi\tau}{N_{rs}}\right), \quad (14) \end{aligned}$$

where  $P$  is the power of the bandpass signal,  $N_{rb} \in \{6, 15, 25, 50, 75, 100\}$  is the number of RBs,  $N_{rs} = 12N_{rb} - 4$ ,  $\theta_{rs} \in \{0, 1, 2, 3, 4, 5\}$  is the subcarrier shift of PRS, and  $\tau$  is in unit of  $T_s = 1/(N_{rs}\Delta f_{sc})$ . Note that the ACF output of PRS has a similar shape to the sinc function and the mainlobe of the ACF output is inversely proportional to  $N_{rb}$ , as shown in Fig. 2, where the horizontal axis is the distance ( $= \tau c$ ). Therefore, multipath with a smaller TOA than  $t_{\text{LOS}} + T_s$  can corrupt the ACF output such that the ACF output of the T-FAP and that of the R-FAP can have peaks appearing at different points, which results in the TOA of R-FAP different from the TOA of T-FAP. In addition, when UE measures the TOA of the R-FAP from discrete ACF output [31], the measured TOA of the R-FAP may be different from the TOA of the R-FAP depending on the employed TOA detection function.

In the following, we analyze the performance of TOA detection function when the R-FAP is constructed by multipath, exploiting the two-path model [9], where individual multipath constituting the R-FAP are categorized into two groups; the first group is a group of paths arriving closely to the LOS path and the second group representing the sum of other later arriving multipath.

In general, CIR of a multipath channel is expressed as

$$h_{\text{all}}(\tau) = \sum_{n=1}^M a_n e^{-j\theta_n} \delta(\tau - \tau_{(n)}), \quad (15)$$

where  $a_n$ ,  $\tau_{(n)}$  and  $\theta_n$  are the magnitude, excess delay, and phase of the individual  $n$ -th arrival path, respectively.

Note that for a path with  $\tau_{(n)} > \tau_{\text{LOS}}$ , the amplitude  $a_n$  follows a Rayleigh distribution [28], and the likelihood distributions of  $a_n^2$  and  $\theta_n$  are an exponential distribution [24] and a uniform distribution in  $[0, 2\pi)$  [32], [33], respectively. Note also that  $\tau$  for small excess delay follows  $f_\tau(\tau)$  (12), which means that a path with a smaller delay is likely to occur more often and is likely to have a higher power. Exploiting the two-path model, there are  $N (\ll M)$  paths constituting the R-FAP, where  $N_1$  individual paths are arriving closely to the T-FAP and  $N_2 (= N - N_1)$  paths are arriving later, so that the CIR for the R-FAP can be found as [9]

$$h(\tau) = \alpha_1 \delta(\tau - \tau_1) + \alpha_2 \delta(\tau - \tau_2), \quad (16)$$

where

$$\alpha_1 \simeq \sum_{n=1}^{N_1} a_n e^{-j\psi_n} \quad (17a)$$

$$\alpha_2 \simeq \sum_{n=N_1+1}^N a_n e^{-j\psi_n} \quad (17b)$$

$$\tau_{(N_1+1)} \leq \tau_2 \leq \tau_{(N)}. \quad (17c)$$

In Rician channels, UE timing is well synchronized to the LOS path that dominates the R-FAP so that  $|\alpha_1| \gg |\alpha_2|$ ,  $\psi_n \simeq \theta_n - \theta_1$ ,  $\alpha_1 \simeq a_1$ ,  $\tau_1 = 0$ , and the net amplitude  $\alpha_2$  follows Gaussian distribution [9], [33]. Therefore, the CIR for the R-FAP in Rician channels can be approximated by

$$h(\tau) \approx \alpha_1 \delta(\tau) = h_1(\tau), \quad (18)$$

when the Rician fading factor is large ( $K \gg 1$ ), so that the ACF output can be found as

$$R_1(\tau) \approx h_1(\tau) * R_L(\tau) = \alpha_1 R_L(\tau), \quad (19)$$

where  $(\cdot)_1$  represents the Rician channel. Applying a matched filter to detect the TOA of the R-FAP from (19), the MI error  $\tau_{m,1}$  of the LTE PRS in Rician channel is negligible, and hence we obtain

$$f_{\tau_{m,1}}(\tau) \simeq \delta(\tau). \quad (20)$$

In Rayleigh channels, on the other hand, we assume that LOS path and multipath arriving closely to the LOS path are severely attenuated due to the obstacles so that the second group is stronger than the first group ( $|\alpha_2| \gg |\alpha_1|$ ) and the UE timing is synchronized to the second group whose delay is  $\tau_2$ . And since the first group and the second group are constructed by a number of multipath,  $\alpha_1$  and  $\alpha_2$  follow Gaussian distribution [33]. Note also that even if the T-FAP is not the LOS path in Rayleigh channels,  $\tau_1 \rightarrow \tau_{(1)}$  for large  $M$ .

Exploiting the analysis of the two-path model in [34], it is found that

$$\begin{aligned} \tau_{m,2} &\simeq \frac{\alpha_2(\tau_2 - \tau_1)}{\alpha_1 \cos(\psi_1) + \alpha_2} \simeq \tau_2 - \tau_1 \\ &\simeq \tau_2 - \tau_{(1)}, \end{aligned} \quad (21)$$

where it is assumed that  $\tau_1 \rightarrow \tau_{(1)}$  for large  $M$  and  $|\alpha_2| \gg |\alpha_1|$ . In [35] and [36], it is found that the difference

between the excess delays of the sequentially arriving clustered multipath follows a Poisson distribution with parameter  $\lambda$  as

$$\begin{aligned} f_{\tau_2 - \tau_1}(\tau) &= f_{\tau_2}(\tau) = \lambda e^{-\lambda\tau} \\ &= f_{\tau_{m,2}}(\tau) \end{aligned} \quad (22)$$

for  $\tau \geq 0$ , where  $\lambda$  is the average arrival rate for each first multipath reflected by clusters [35]. Note that the MI error PDF  $f_{M,2}(\tau)$  (22) can have a narrow distribution when UE is equipped with a super-resolution (SR) technique [13]–[15] and when there are enough number of signal samples with sufficiently high SNR. However, these conditions are not always met in practice, and many UEs use matched filter-based path detection technique [12] due to the low computational cost. As a result,  $f_{M,2}(\tau)$  (22) can be used as a general MI error PDF in Rayleigh channels.

### C. Noise Error PDF

In general, the accuracy of the TOA detection function degrades when noise power increases. The performance of the TOA detection function for LTE PRS is degraded with a decreased SNR, as found in [27]. Therefore, in addition to the excess delay of the T-FAP  $\tau_{(1)}$  (12) and the MI error  $\tau_m$  (20) and (21), the final TOA detection is further degraded by the noise  $n(\tau)$  in the discrete ACF output of the R-FAP, as discussed with (5).

The noise error PDF  $f_{\tau_n}(\tau)$  is the distribution of the measured TOA error due to the noise  $n(\tau)$  when UE employs a matched filter to detect the TOA of the incoming signal [12], [26]

$$f_{\tau_n}(\tau) = \mathcal{N}(0, \sigma_n^2), \quad (23)$$

where the Cramér-Rao Bound (CRB) of the noise,  $\text{CRB}_n$ , is found [27] so that

$$\sigma_n^2 \geq \text{CRB}_n = \frac{T_y^2}{8\pi^2\gamma \sum_{n \in \mathcal{N}_a} p(n)^2 n^2}, \quad (24)$$

$T_y = 1/\Delta f_{sc}$ ,  $N_a$ ,  $p(n)$ , and  $\gamma$  denote the OFDM symbol period, set of available pilot subcarriers, and relative power weights satisfying

$$\sum_{n=0}^{N_{sc}} p(n)^2 = 1, \quad (25)$$

and SNR, respectively, and  $N_{sc}$  denotes the number of subcarriers. In the following, we assume  $\sigma_n^2 = \text{CRB}_n$  for UEs using signal processing techniques to improve the matched filter [12].

## IV. OVERALL TOA ERROR DISTRIBUTION

In this section, we build the overall TOA error distribution model for Rician and Rayleigh channels by integrating PDFs for T-FAP error, MI error, and noise error found in Section III.

### A. Rician Channel

Since the TOA errors due to the noise, the NLOS propagation, and MI are mutually independent, the overall TOA error PDF of the R-FAP in a noisy Rician channel is found as

$$\begin{aligned} f_{\tau_o,1}(\tau) &\simeq f_{\tau,1}(\tau) * f_{\tau_n}(\tau) \\ &\simeq f_{\tau_{(1)},1}(\tau) * f_{\tau_m,1}(\tau) * f_{\tau_n}(\tau) \\ &\simeq f_{\tau_n}(\tau) \\ &\simeq \mathcal{N}(0, \sigma_n^2), \end{aligned} \quad (26)$$

where  $\tau_o$  is the TOA, the measured excess delay, of the R-FAP, and  $\sigma_n^2$  is in (24).

### B. Rayleigh Channel

The TOA of the R-FAP in a Rayleigh channel is not as simple as (26). Using (12) and (13), the TOA error PDF of the T-FAP

$$\begin{aligned} f_{\tau_{(1)},2}(\tau) &= f_{\tau_{(1)}}(t)|_{t=D/c+\tau} \\ &= M[1 - F_\tau(\tau)]^{M-1} f_\tau(\tau), \end{aligned} \quad (27)$$

where  $F_\tau(\tau)$  and  $f_\tau(\tau)$  are the CDF and PDF of the excess delay in Rayleigh channel, respectively, can be simplified to

$$f_{\tau_{(1)},2}(\tau) \approx \frac{M}{\sigma_c \sqrt{2}} \left(\frac{1}{2}\right)^{\frac{M}{2}} \left(\frac{1}{\pi}\right)^M \exp\left(-\frac{(M+1)\tau^2}{32\sigma_c^2}\right) \quad (28)$$

for small excess delay  $\tau$ . Note that when  $M$  is large, as in most urban environments,  $f_{\tau_{(1)},2}(\tau)$  has most of the density near the zero excess delay [8]. With the assumption that  $M$  is large enough, we approximate  $f_{\tau_{(1)},2}(\tau)$  by a normal distribution with a very small positive mean as

$$f_{\tau_{(1)},2}(\tau) \approx \mathcal{N}\left(\mu_{\tau_{(1)}}, \sigma_{\tau_{(1)}}^2\right), \quad (29)$$

where

$$\mu_{\tau_{(1)}} \simeq 8\sqrt{2}\sigma_c \frac{M}{M+1} \left(\frac{1}{2\pi}\right)^{M/2} \quad (30a)$$

$$\begin{aligned} \sigma_{\tau_{(1)}}^2 &\simeq \int_0^\infty (\tau - \mu_{\tau_{(1)}})^2 \\ &\quad \times \frac{M}{\sigma_c \sqrt{2}} \left(\frac{1}{2\pi}\right)^{\frac{M}{2}} \exp\left(-\frac{(M+1)\tau^2}{32\sigma_c^2}\right) d\tau \end{aligned} \quad (30b)$$

are the mean and variance of  $f_{\tau_{(1)},2}(\tau)$  (29) [37]. Therefore, the overall TOA error PDF of R-FAP in a noisy Rayleigh channel is found as

$$\begin{aligned} f_{\tau_o,2}(\tau) &= f_{\tau_{(1)},2}(\tau) * f_{\tau_m,2}(\tau) * f_{\tau_n}(\tau) \\ &\simeq \frac{\lambda}{\pi} \left(2\mu_{\tau_{(1)}} + \lambda(\sigma_{\tau_{(1)}} + \sigma_n^2) - 2\tau\right) \int_\infty^\tau e^{-\tau^2} d\tau \\ &\simeq \frac{\lambda}{2\sqrt{2\pi}} \left(2\mu_{\tau_{(1)}} + \lambda(\sigma_{\tau_{(1)}} + \sigma_n^2) - 2\tau\right) e^{-\tau^2/4}. \end{aligned} \quad (31)$$

Using [38], the respective mean and variance of the TOA errors (31) in Rayleigh channels are found as

$$\mu_{\tau_o} \simeq \mu_{\tau_{(1)}} + \frac{1}{\lambda} \quad (32a)$$

$$\sigma_{\tau_o}^2 \simeq \sigma_{\tau_{(1)}}^2 + \sigma_n^2 + \frac{1}{\lambda}. \quad (32b)$$

Note that from (32a), (32b), (30a), and (30b), the mean TOA error in Rayleigh channel depends on  $\sigma_c$  (function of  $D$ ), and  $\lambda$ , which is determined by the scattering environments, and that the variance of the TOA error in Rayleigh channel depends not only on  $M$ ,  $\sigma_c$ , and  $\lambda$ , but also on the  $\sigma_n$  (function of signal bandwidth and SNR).

## V. OVERALL TDOA ERROR DISTRIBUTION

In this section, we derive closed-form expressions for the TDOA error PDF discussed in Section II utilizing the TOA error PDF in Section IV, and the derived expressions are verified with histograms obtained from numerous Monte Carlo simulations. Let  $d\tau_o^{(n,s)}$  be the TDOA between a neighbor ENB (ENB<sub>n</sub>) and the service ENB (ENB<sub>s</sub>), which is obtained from the TOA of the ENB<sub>n</sub> minus the TOA of the ENB<sub>s</sub>, i.e.,  $\tau_o^{(n)} - \tau_o^{(s)}$ . In the Monte Carlo simulations, the path delays are obtained by computing the distance of  $M$  downlink paths scattered at randomly located  $M$  scatterers from a circular Gaussian distribution with  $\sigma_c$  ( $= 0.337D/c$ ) around the UE, and the SNR is 20dB, where  $M$  is uniformly random in  $U[25, 35]$ . For Rician channels, the LOS path is amplified to have a much larger power than other multipath, while for Rayleigh channels, the path loss model introduced in [39] is applied to each path. Matched filter technique [40] is applied to the discrete ACF output to estimate the TOA of the R-FAP.

### A. Rician-Rician Channel

Since the TOA error PDF in Rician channel is approximated by normal distribution, the TDOA error PDF when both downlinks have Rician channel is found as

$$\begin{aligned} f_{d\tau_o,1}^{(n,s)}(\tau) &= f_{\tau_o,1}^{(n)}(\tau) * f_{\tau_o,1}^{(s)}(-\tau) \\ &\simeq \mathcal{N}\left(0, \sigma_n^{(s)2} + \sigma_n^{(n)2}\right) \end{aligned} \quad (33)$$

where  $(\cdot)^{(n,s)}$   $(\cdot)^{(n)}$  and  $(\cdot)^{(s)}$  represent the difference between ENB<sub>n</sub> and ENB<sub>s</sub>, ENB<sub>n</sub>, and ENB<sub>s</sub>, respectively. Fig. 3 shows  $f_{d\tau_o,1}^{(n,s)}(\tau)$  for GSMD and TDOA error histogram obtained with numerous Monte Carlo simulations for downlink GSMD. As shown, we can observe that the theoretical TDOA error PDF agrees with the TDOA error histogram obtained with  $10^4$  Monte Carlo simulations, and both of them becomes narrower for larger bandwidth ( $N_{rb}$ ) of the LTE PRS signal and have zero-means.

### B. Rayleigh-Rayleigh Channel

The principle expression for the TDOA error PDF is defined in (6). The TDOA error PDF of the T-FAPs between ENB<sub>n</sub> and ENB<sub>s</sub> when both downlinks have Rayleigh channel is found as

$$\begin{aligned} f_{d\tau_{(1)},2}^{(n,s)}(\tau) &= f_{\tau_{(1)}}^{(n)}(\tau) * f_{\tau_{(1)}}^{(s)}(-\tau) \\ &\simeq \mathcal{N}\left(\mu_{\tau_{(1)}}^{(n)} - \mu_{\tau_{(1)}}^{(s)}, \sigma_{\tau_{(1)}}^{(n)2} + \sigma_{\tau_{(1)}}^{(s)2}\right). \end{aligned} \quad (34)$$

The PDF of the difference between the noise error in the TOA of the ENB<sub>n</sub> and that of the ENB<sub>s</sub> is expressed as

$$\begin{aligned} f_{d\tau_n}^{(n,s)}(\tau) &= f_{\tau_n}^{(n)}(\tau) * f_{\tau_n}^{(s)}(-\tau) \\ &= \mathcal{N}\left(0, \sigma_n^{(s)2} + \sigma_n^{(n)2}\right), \end{aligned} \quad (35)$$

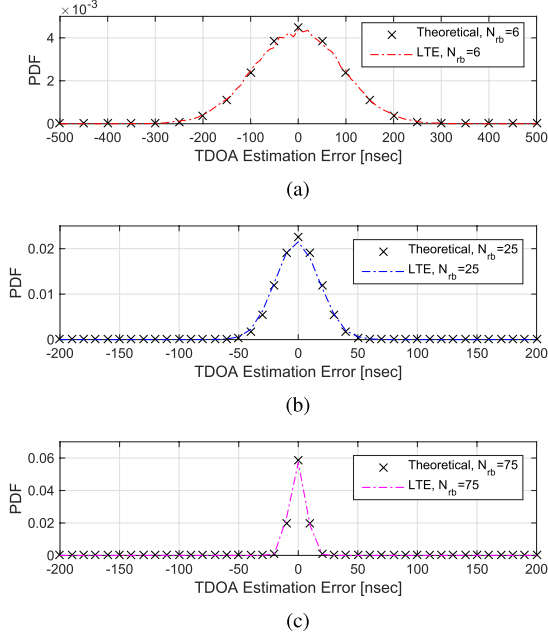


Fig. 3. TDOA error distributions for Rician-Rician channels. (a)  $N_{rb} = 6$ . (b)  $N_{rb} = 25$ . (c)  $N_{rb} = 75$ .

and the PDF of the difference between the MI error in TOA of the ENB<sub>n</sub> and that of the ENB<sub>s</sub> is obtained as

$$\begin{aligned} f_{d\tau_m,2}^{(n,s)}(\tau) &= f_{\tau_m,2}^{(n)}(\tau) * f_{\tau_m,2}^{(s)}(-\tau) \\ &= \frac{\lambda}{2} e^{-\lambda|\tau|} \end{aligned} \quad (36)$$

Using (34), (35), and (36), we obtain the TDOA error PDF of the R-FAP when both downlinks have noisy Rayleigh channel as

$$\begin{aligned} f_{d\tau_o,2}^{(n,s)}(\tau) &= f_{\tau_o,2}^{(n)}(\tau) * f_{\tau_o,2}^{(s)}(-\tau) \\ &= \mathcal{N}\left(\mu_{\tau_{(1)}}^{(n)} - \mu_{\tau_{(1)}}^{(s)}, \sigma_{\tau_{(1)}}^{(n)2} + \sigma_{\tau_{(1)}}^{(s)2} + \sigma_n^{(n)2} + \sigma_n^{(s)2}\right) \\ &\quad * f_{\tau_m}(\tau) * f_{\tau_m}(-\tau). \end{aligned} \quad (37)$$

The closed-form expression for  $f_{d\tau_o,2}^{(n,s)}(\tau)$  (37) is difficult to obtain; however, the mean and approximate variance of the TDOA following  $f_{d\tau_o,2}^{(n,s)}(\tau)$  can be found utilizing the variance of  $f_{\tau_m}(\tau) * f_{\tau_m}(-\tau)$  as

$$\mu_{d\tau_o,2}^{(ns)} \simeq \mu_{\tau_{(1)}}^{(n)} - \mu_{\tau_{(1)}}^{(s)} \quad (38a)$$

$$\sigma_{d\tau_o,2}^{(ns)2} \simeq \sigma_{\tau_{(1)}}^{(n)2} + \sigma_{\tau_{(1)}}^{(s)2} + \sigma_n^{(n)2} + \sigma_n^{(s)2} + \frac{1}{\lambda^2}, \quad (38b)$$

respectively. Notice that the mean of TDOA error  $\mu_{d\tau_o,2}^{(ns)}$  is not always zero, since  $\mu_{\tau_{(1)}}$  (30a) depends on  $M$  and  $\sigma_c$  of the downlink channel (however, a large  $M$  is not a dominant factor), where  $\sigma_c$  is a function of downlink distance  $D$  [25], [30]. For example, when a UE is closer to ENB<sub>s</sub> than ENB<sub>n</sub>,  $\sigma_c^{(s)}$  becomes smaller than  $\sigma_c^{(n)}$ , which results in a larger positive mean of TDOA error  $\mu_{d\tau_o,2}^{(ns)}$ . This agrees with general intuition that a UE may observe small excess delays in TOA measurements when the UE is closer to an ENB than when the UE is far away from an ENB.

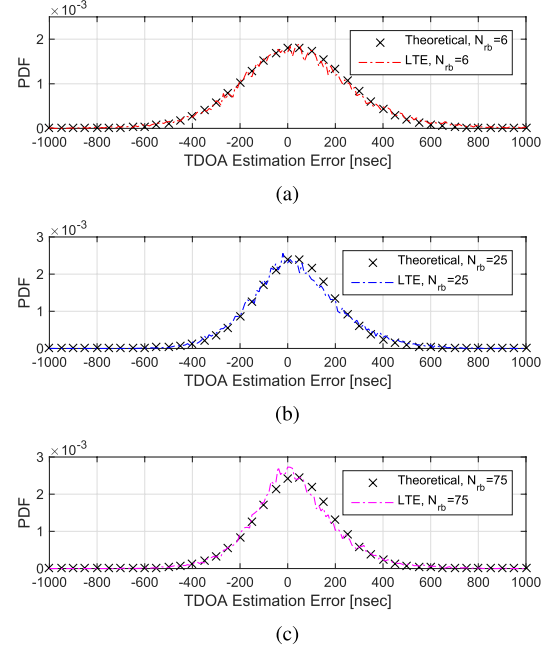


Fig. 4. TDOA error distributions for Rayleigh-Rayleigh channels and  $[D^{(s)}, D^{(n)}] = [200, 1400]\text{m}$ . (a)  $N_{rb} = 6$ . (b)  $N_{rb} = 25$ . (c)  $N_{rb} = 75$ .

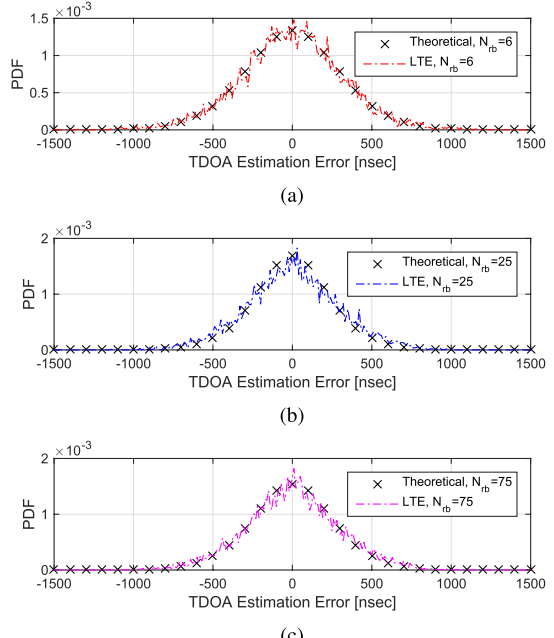
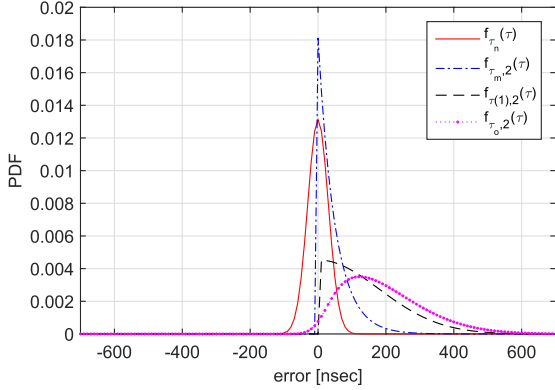
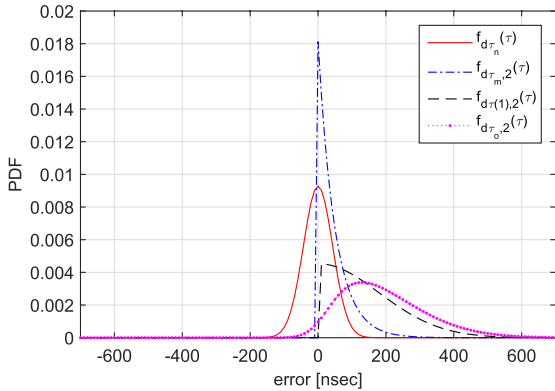


Fig. 5. TDOA error distributions for Rayleigh-Rayleigh channels and  $[D^{(s)}, D^{(n)}] = [800, 800]\text{m}$ . (a)  $N_{rb} = 6$ . (b)  $N_{rb} = 25$ . (c)  $N_{rb} = 75$ .

Similar to the results shown in Fig. 3, Fig. 4 and Fig. 5 show good agreements between the theoretical expression  $f_{d\tau_o,2}^{(n,s)}(\tau)$  (37) and the TDOA error histogram obtained from  $10^4$  Monte Carlo simulations. In Fig. 4 and Fig. 5, we test two scenarios; when a UE is located relatively very close to ENB<sub>s</sub>:  $[D^{(s)}, D^{(n)}] = [200, 1400]\text{m}$ , and when a UE is located in the middle of the ENB<sub>s</sub> and ENB<sub>n</sub>:  $[D^{(s)}, D^{(n)}] = [800, 800]\text{m}$ . As shown, the TDOA error histogram becomes narrower for larger bandwidth ( $N_{rb}$ ) of the PRS, and the theoretical

Fig. 6. TOA error components for  $N_{rb} = 25$  case in Fig. 4.Fig. 7. TDOA error components for  $N_{rb} = 25$  case in Fig. 4.

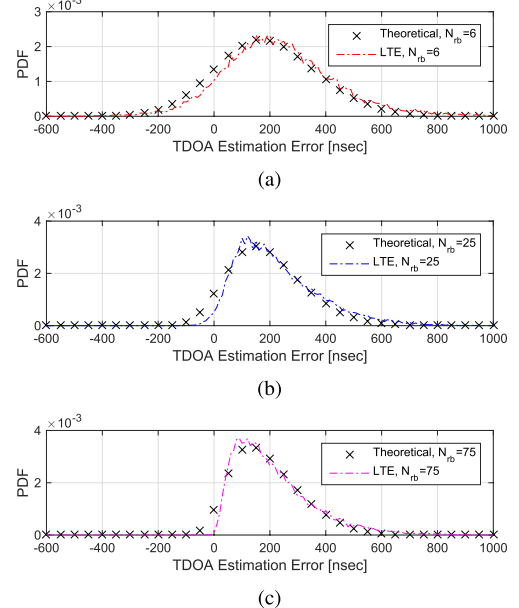
TDOA error PDF matches the TDOA error histogram. In Fig. 4 and Fig. 5, we use  $\sigma_c \simeq 0.33D/c$  for urban environments [25], [30]. As expected with  $\mu_{\tau_{(1)}}^{(n)} > \mu_{\tau_{(1)}}^{(s)}$ , we can observe the positive mean of the TDOA error PDF and the positive mean of the TDOA error histogram in Fig. 4, but  $\mu_{\tau_{(1)}}^{(n)} = \mu_{\tau_{(1)}}^{(s)}$  in Fig. 5.

Fig. 6 shows the TOA error components (i.e., noise, MI error, and T-FAP errors) contributing to the TDOA error shown in Fig. 4, and Fig. 7 shows the difference between the same TOA error components. By comparing the results in Fig. 6 and Fig. 7, we observe that all of the TOA error components contribute to the TDOA error, since none of them is negligibly small (i.e., zero-mean and relatively narrow distribution).

### C. Rayleigh-Rician Channel

When one downlink (e.g., downlink from ENB<sub>s</sub>) has a Rician channel and the other downlink (e.g., from ENB<sub>n</sub>) has a Rayleigh channel, the TDOA error PDF can be found as follows. The TDOA error PDF of the T-FAP between ENB<sub>n</sub> and ENB<sub>s</sub> is expressed as

$$f_{d\tau_{(1)},2,1}^{(n,s)}(\tau) = f_{\tau_{(1)},2}^{(n)}(\tau) * f_{\tau_{(1)},1}^{(s)}(-\tau) \simeq \mathcal{N}\left(\mu_{\tau_{(1)}}^{(n)}, \sigma_{\tau_{(1)}}^{(n)2}\right), \quad (39)$$

Fig. 8. TDOA error distributions for Rayleigh-Rician channels and  $[D^{(s)}, D^{(n)}] = [200, 1400]$ m. (a)  $N_{rb} = 6$ . (b)  $N_{rb} = 25$ . (c)  $N_{rb} = 75$ 

where  $(\cdot)_{:,2,1}^{(n,s)}$  represents that ENB<sub>n</sub> signal has a Rayleigh channel and ENB<sub>s</sub> has a Rician channel. The PDF of the difference between the noise error in the TOA of the ENB<sub>n</sub> and that of the ENB<sub>s</sub> is

$$f_{d\tau_n}^{(n,s)}(\tau) = f_{\tau_n}^{(n)}(\tau) * f_{\tau_n}^{(s)}(-\tau) = \mathcal{N}\left(0, \sigma_n^{(n)2} + \sigma_n^{(s)2}\right), \quad (40)$$

and the PDF of the difference between the MI error in the TOA of the ENB<sub>n</sub> and that of the ENB<sub>s</sub> is obtained as

$$f_{d\tau_{m,2},1}^{(n,s)}(\tau) = f_{\tau_{m,2}}^{(n)}(\tau) * f_{\tau_{m,1}}^{(s)}(-\tau) \times \begin{cases} \lambda e^{-\lambda\tau}, & \text{for } \tau \geq 0 \\ 0, & \text{for } \tau < 0. \end{cases} \quad (41)$$

Using (39), (40), and (41), we derive the TDOA error PDF of the R-FAP when ENB<sub>n</sub> downlink has a noisy Rayleigh channel and ENB<sub>s</sub> downlink has a noisy Rician channel as

$$f_{d\tau_{o,2},1}^{(n,s)}(\tau) = f_{\tau_{o,2}}^{(n)}(\tau) * f_{\tau_{o,1}}^{(s)}(-\tau) = \mathcal{N}\left(\mu_{\tau_{(1)}}^{(n)}, \sigma_{\tau_{(1)}}^{(n)2} + \sigma_n^{(s)2} + \sigma_n^{(n)2}\right) * f_{\tau_{o,2}}(\tau). \quad (42)$$

The closed form expression for (42) is difficult to find; however, the mean and the approximate variance of (42) can be found as

$$\mu_{d\tau_{o,2},1}^{(n,s)} \simeq \mu_{\tau_{(1)}}^{(n)} + \frac{1}{\lambda} \quad (43a)$$

$$\sigma_{d\tau_{o,2},1}^{(n,s)2} \simeq \sigma_{\tau_{(1)}}^{(n)2} + \sigma_n^{(s)2} + \sigma_n^{(n)2} + \frac{1}{\lambda^2} \quad (43b)$$

Fig. 8 shows the TDOA error PDFs and histograms when PRS from ENB<sub>s</sub> has a Rician channel and that from ENB<sub>n</sub> has a Rayleigh channel. Since both the MI error and the TOA error of the T-FAP are positive in Rayleigh channel, and the TOA error PDF in Rician channel is approximated by a zero-mean

TABLE I  
 $\mathcal{D}_{\text{RMSE}}\{p_1, p_2\}$  FOR THEORETICAL AND SIMULATED  
 PMF IN FIG. 3, FIG. 4, FIG. 5, AND FIG. 8

Fig. num.	$N_{rb} = 6$	$N_{rb} = 25$	$N_{rb} = 75$
Fig. 3	$0.0551 \times 10^{-3}$	$0.1561 \times 10^{-3}$	$0.2417 \times 10^{-3}$
Fig. 4	$0.5314 \times 10^{-4}$	$0.7765 \times 10^{-4}$	$0.8663 \times 10^{-4}$
Fig. 5	$0.5696 \times 10^{-4}$	$0.9565 \times 10^{-4}$	$0.7138 \times 10^{-4}$
Fig. 8	$0.0978 \times 10^{-3}$	$0.1340 \times 10^{-3}$	$0.1327 \times 10^{-3}$

Gaussian distribution, the TDOA error PDFs and histograms shown in Fig. 8 have most of the density in the positive TDOA values, which reveals that there is a non-negligible positive mean TDOA offset. This can lead to a large positioning error in practice.

The theoretical expression and histograms are compared using the following equation for Fig. 3, Fig. 4, Fig. 5, and Fig. 8 to decide if they are well-matched [41],

$$\mathcal{D}_{\text{RMSE}}\{p_1, p_2\} = \left[ \frac{1}{|\mathcal{X}|} \sum_{i \in \mathcal{X}} |p_1(i) - p_2(i)|^2 \right]^{1/2}, \quad (44)$$

where  $p_1$  and  $p_2$  are two possible probability mass function (PMF) representing a random variable (RV) taking values on a set  $\mathcal{X}$ . The results summarized in Table I verifies the goodness of the approximation.

#### D. Comparison to the Conventional Channel Models

The TOA and TDOA error PDFs derived in this paper provide some novel contributions to the positioning channel models. First, the TOA error PDF found in this paper is based on geometrically-based statistical (theoretical) scatterer distribution, where the spread of scatterer distribution increases with the downlink distance, and, thus, TOA delay spreads increases with the downlink distance. On the contrary, EPA, EVA, and ETU models have multipath with fixed-delays and independent fading [17] so that while their R-FAPs have varying TOA delays, their T-FAPs have always the same fixed delay. This may be not an appropriate model for positioning channel. In the WINNER model for outdoor multipath environments, on the other hand, the delay spread (large scale parameter) follows a log-normal distribution with a fixed mean and variance based on empirical observations [18]. Given the delay spread, the width of the exponentially distributed TOA (small scale parameter) error PDF is determined. The delay spread is randomly determined regardless of UE's location in the cell so that UEs in the vicinity of ENB and UEs at the cell edge can have similar TOA distribution when averaged over all probable delay spreads. Second, the TOA error PDF derived in this paper provides the error distribution of the measured TOA (i.e., TOA error of R-FAP) and that of the measured TDOA between R-FAPs, using the matched filter-based path detection technique [12] for PRS that has various signal bandwidth, channel condition, and SNR. In contrast, the conventional TOA error PDF only considers multipath delays, fading of the each path components, and the effect of noise, so that the effect of multipath interference, signal bandwidth, and channel condition are not included. In addition, the conventional models cannot provide any expression for the

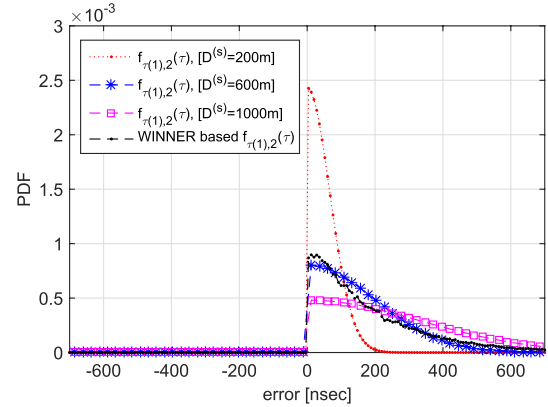


Fig. 9. TOA error distributions of T-FAP.

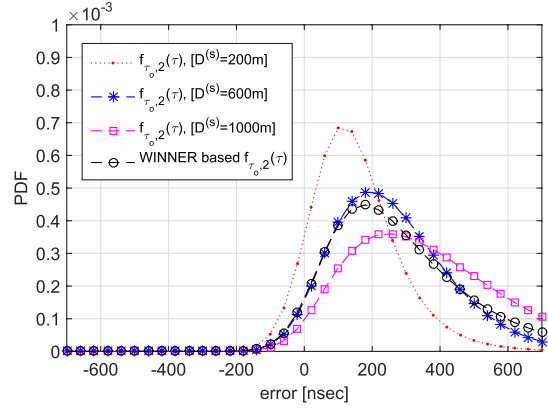


Fig. 10. TOA error distributions of R-FAP.

TOA and TDOA error distribution of the R-FAP. Third, the conventional TOA error models are inappropriate to generate TDOA errors for positioning simulations. The T-FAP of the EPA/EVA/ETU TOA error models has a fixed delay, so that their TDOAs have zero mean regardless of the UE environments, UE location, and signal waveform. This is similar to the WINNER model, where the width of TOA error distribution for a site depends on a randomly chosen delay spread that has a log-normal distribution. Therefore, when the TOA error distribution is averaged over all probable delay spreads, any UE at any location in a cell should have the same TOA distribution, which results in a zero-mean TDOA. However, the TDOA error PDF derived in this paper has a non-zero mean error depending on the relative downlink distance.

To compare the TOA error PDF derived in this paper to the WINNER model (in C1 Metropol Scenario), we compare the TOA error PDF of T-FAP  $f_{\tau(1),2}(\tau)$  that does not include MI and noise errors for various downlink distance. The Fig. 9 shows the TOA error histogram of the T-FAP from the WINNER model and  $f_{\tau(1),2}(\tau)$  for UEs at downlink distance 200m, 600m, and 1000m and  $N_{rb} = 25$ . The TOA error histogram of the T-FAP from the WINNER model is averaged for all probable delay spreads so that the TOA error histogram of the T-FAP for WINNER model in Fig. 9 has a fixed distribution, whereas  $f_{\tau(1),2}(\tau)$  has wide (narrow) distribution when  $D^{(s)}$  is large (small). Note that the TOA error histogram

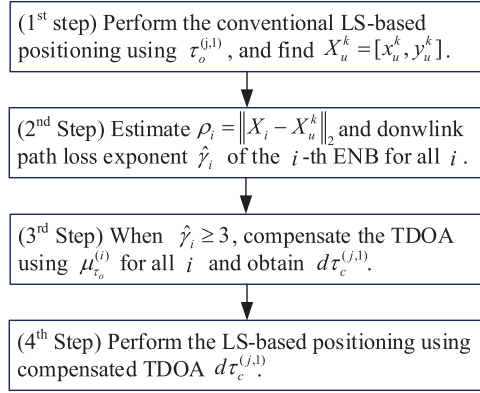


Fig. 11. Proposed TDOA positioning technique.

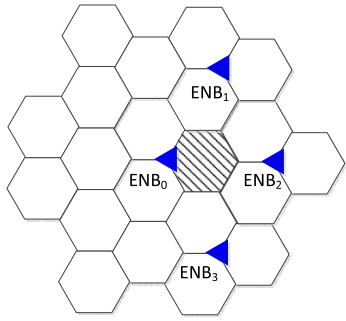


Fig. 12. ENB locations (blue triangles) and possible locations of UE (shaded area). Neighboring ENBs are at 1km distance.

of the T-FAP for the WINNER model and  $f_{\tau(1),2}(\tau)$  for  $D^{(s)} = 600\text{m}$  are very similar in Fig. 9. The Fig. 10 shows the TOA error PDF of R-FAP,  $f_{\tau_o,2}(\tau)$ , by integrating MI and noise errors into the  $f_{\tau(1),2}(\tau)$  for  $N_{rb} = 25$ . For  $D^{(s)} = 600\text{m}$ , we have found that the WINNER model and the theoretical expression,  $f_{\tau_o,2}(\tau)$ , derived in this paper have a very similar distribution. However, the WINNER model has a fixed distribution when averaged over all probable delay spreads, whereas  $f_{\tau_o,2}(\tau)$  can have a wider (narrower) distribution for large (small)  $D^{(s)}$  than the WINNER model.

## VI. TDOA PERFORMANCE IMPROVEMENT IN LTE

In this Section, we propose a TDOA positioning technique that compensates the mean TDOA error to improve OTDOA positioning accuracy in LTE systems. We demonstrate the performance improvement with Monte Carlo simulations.

### A. Proposed TDOA Positioning Technique

The proposed TDOA positioning technique consists of four steps as illustrated in Fig. 11. In the first step, an initial position estimate of UE  $X_u^0 = [x_u^0, y_u^0]^T$  is obtained using the conventional LS-based TDOA positioning algorithm [42] with the TDOA measurements  $d\tau_o^{(n,s)}$ , where  $(\cdot)^T$  represents the matrix transpose [28]. When the uncertainty weight matrix  $R$  is an identity matrix, the LS-based TDOA positioning algorithm [42] minimizes the cost function

$$J = \frac{1}{2}(Z - H\Delta X)^T R^{-1}(Z - H\Delta X), \quad (45)$$

iteratively, and the location update at the  $k$ -th iteration is

$$\Delta X^{k-1} = [\Delta x^{k-1}, \Delta y^{k-1}]^T = (H^T R^{-1} H)^{-1} H^T R^{-1} Z, \quad (46)$$

where the  $l$ -th row ( $l \in \{1, 2, \dots, N_e - 1\}$ ) of  $H$  and  $l$ -th element of  $Z$  are

$$H_l = \left[ \frac{(x_{l+1} - x_u^k)}{\rho_{l+1}^k} - \frac{(x_1 - x_u^k)}{\rho_1^k}, \frac{(y_{l+1} - y_u^k)}{\rho_{l+1}^k} - \frac{(y_1 - y_u^k)}{\rho_1^k} \right], \quad (47)$$

$$Z[l] = \left[ \rho_{l+1}^k - \rho_1^k - c \times d\tau_o^{(l+1,1)} \right], \quad (48)$$

respectively,  $X_i = [x_i, y_i]^T$  represents the location of the  $i$ -th ENB for  $i \in \{1, 2, \dots, N_e\}$ ,  $\rho_i^k$  represents the Euclidian distance between  $[x_i, y_i]$  and the UE position estimate,

$$X_u^k = X_u^{k-1} + \Delta X^{k-1}, \quad (49)$$

$N_e$  is the total number of ENBs whose PRS is measured, and  $d\tau_o^{(j,1)}$  ( $j \in \{2, 3, \dots, N_e\}$ ) is the measured TDOA using the measured TOA of the  $j$ -th ENB,  $\tau_{(1)}^{(j)}$ , and that of the first (i.e., service) ENB,  $\tau_{(1)}^{(1)}$ . The procedure from (46) to (49) is repeated until  $|\Delta X^{k-1}|$  becomes small enough. Note that in the conventional weighted LS (WLS)-based TDOA positioning algorithms  $R$  is the uncertainty matrix whose diagonal elements can be the measurement noise variance [42]. In the second step, we obtain downlink distance estimates  $\rho_i$  for all ENBs using  $X_u^k$  from the first step. Then, UE tests each downlink to determine whether the downlink is from Rician channel or Rayleigh channel based on  $\rho_i$  and the received signal strength of the downlink  $P_i$ . Since system information block-2 (SIB2) from each ENB contains the transmission power of reference signal (RS) at ENB and PRS-RA (PRS-to-RS energy per resource element ratio) is available to UE [43], UE can estimate the path loss of the downlink using an appropriate path-loss model. In the simulations, we use a simplified path-loss model [33] to estimate the path-loss exponent as

$$\hat{\gamma}_i = \frac{1}{10\log_{10}\rho_i} (P_i^t - P_{i,\text{dBm}} + K_{\text{dB}}), \quad (50)$$

where  $P_i^t$  is the transmission power of the PRS at the  $i$ -th ENB,  $K_{\text{dB}} = 20\log_{10}(\lambda/(4\pi d_0))$ ,  $\lambda$  is the carrier wavelength, and  $d_0$  is the reference distance for the antenna far field. Note that the path loss can be estimated using different propagation models such as [39]. In the third step, UE compensates the measured TOA for the expected mean TOA error of the R-FAP,  $\mu_{\tau_o,2}$ , when the TOA measurement is found to be from a Rayleigh channel; the TDOA mean is estimated using  $\mu_{d\tau_o,2}^{(n,s)}$  (38a) with an assumption that  $M = 25$ . In the simulations, we use  $M$  uniformly distributed within  $U[15, 25]$  for moderate multipath environments and  $U[25, 35]$  for severe multipath environments. When the mean of each TDOA measurement is compensated, we obtain the mean compensated TDOA,  $d\tau_c^{j,1}$ , as

$$d\tau_c^{(j,1)} = d\tau_o^{(j,1)} - \mu_{d\tau_o,2}^{(j,1)}, \quad (51)$$

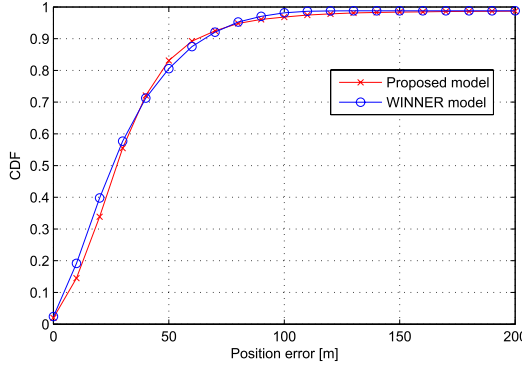


Fig. 13. Comparison of positioning performance for outdoor macro-only deployment scenario in TR37.857.

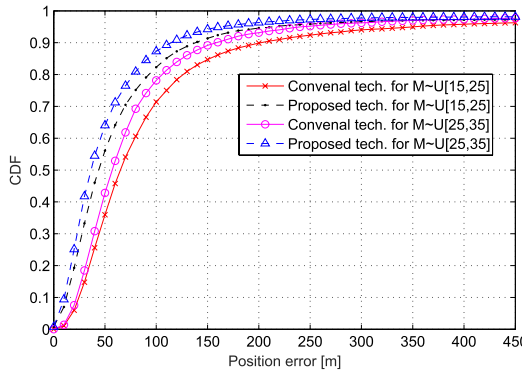


Fig. 14. Positioning performance improvement with the proposed technique for Rayleigh-Rician channels.

where  $\mu_{d\tau_o,2}^{(j,1)}$  denotes the expected TDOA between the  $i$ -th ENB and the first ENB. Finally in the fourth step, the conventional LS-based positioning algorithm [42] is used again with the mean-compensated TDOAs to obtain an improved location estimate of the UE.

### B. Simulation Results

In the following simulations, we assume that ENBs have 3 regular hexagonal cells of the same size, as shown in Fig. 12, and all ENB PRSs have the same transmission power and the same bandwidth, which are known to UEs. We also assume that UEs are uniformly distributed in the service cell area (shaded area in Fig. 12).

In addition to the comparison of TDOA error PDF in Fig. 10, we perform  $10^4$  Monte Carlo simulations of TDOA positioning for UEs uniformly distributed in the service cell as shown in Fig. 12 in order to compare  $f_{d\tau_o}(\tau)$ , the TDOA error of R-FAP, and the TDOA error with the WINNER model [7] in the position-domain. In the simulations, we test the outdoor macro-only deployment scenario (i.e., no outdoor small cells) [44], where the inter-site distance (ISD) is 500m, we use  $M \sim U[15, 25]$  (i.e.,  $M$  is uniformly distributed from 15 to 25),  $\lambda = 100\text{ns}$  [45], SNR= 20dB,  $N_{rb} = 50$ , and  $\sigma_c = 0.33D/c$  to generate the TDOA errors of the R-FAP, and we utilize the propagation model in [39] to determine the received signal strength, where the path loss exponent  $\gamma = 3.5$  is fixed.

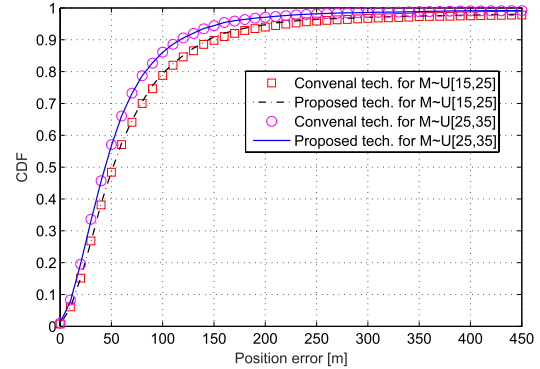


Fig. 15. Positioning performance improvement with the proposed technique for Rayleigh-Rayleigh channels.

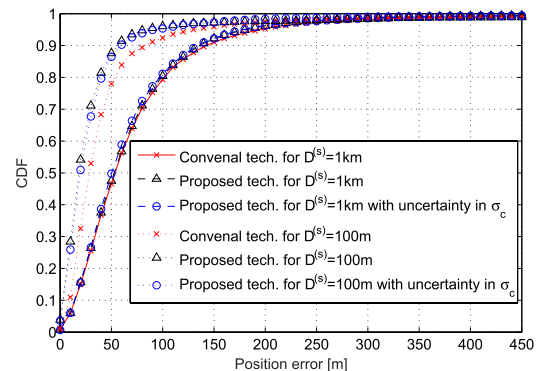


Fig. 16. Positioning performance for  $M \sim U[15, 25]$  with 33% uncertainty in  $\sigma_c$  and LOS probability considered.

is fixed. In addition, we employ a weighted-LS (WLS)-based positioning technique, where the variance of the  $(l+1)$ -th ENB PRS is used for  $R[l,l]$  in (46), and we assume that ENBs use muting to minimize the inter-cell interference during the positioning occasion. The resulting TDOA positioning performance shown in Fig. 13 is very similar to those introduced in [44], where 40m and 80m horizontal positioning accuracies are achieved for about 70% ~ 80% and 95%, respectively. Note that  $\lambda = 100\text{ns}$  and  $\sigma_c = 0.33D/c$  are fixed for the given urban environments, however, we expect that  $M > 25$ ,  $\text{SNR} > 20\text{dB}$ ,  $\lambda < 100\text{ns}$ , and  $\sigma_c < 0.33D/c$  result in a narrower TDOA error PDF and, thus, a better TDOA positioning performance than the result shown in Fig. 13.

In the following simulations, we assume that ISD is 1.5km (large cell size) and UEs are able to detect  $N_e = 4$  ENB signals: one from ENB<sub>s</sub> (=ENB<sub>1</sub>) and three from other ENB<sub>n</sub>'s (i.e., ENB<sub>2</sub>, ENB<sub>3</sub>, ENB<sub>4</sub>). We use  $N_{rb} = 25$ ,  $\lambda = 100\text{ns}$  [45], SNR= 20dB,  $\sigma_c = 0.33D/c$ , and the propagation model in [39] to determine the received signal strength, where the path loss exponent  $\gamma = 3.5$  is fixed.

Fig. 14 and Fig. 15 show the positioning performance improvement with the proposed (TDOA positioning) technique in comparison to the conventional LS-based (TDOA positioning) technique [42]. In the simulations, there are 100 positioning trials at each of 200 uniformly distributed test locations within the service cell. We use  $M \sim U[25, 35]$  and  $M \sim U[15, 25]$  for severe multipath environments and

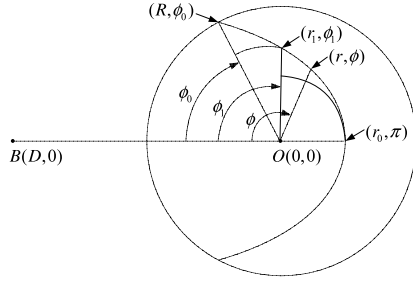


Fig. 17. Area segments for TOA error CDF evaluation used in [8].

moderate multipath environments, respectively. As expected for larger  $M$ , the performance of the proposed algorithm and the conventional algorithm is improved, respectively, since the TOA error of T-FAP has a narrower distribution (i.e., smaller error). The simulation results in Fig. 14 are for a case that PRS of ENB<sub>s</sub> has a Rician channel and others have Rayleigh channels, and those in Fig. 15 are for a different case that all of the PRSs are from Rayleigh channels. As shown in Fig. 4 and Fig. 8, where TDOA between two PRSs from a Rician channel and a Rayleigh channel has a non-zero mean TDOA offset, the results in Fig. 14 shows that the proposed technique provides strong performance improvement. This demonstrates that the knowledge of TDOA error distribution is useful to improve positioning accuracy. However, in the conventional techniques a TDOA from a Rician channel and a Rayleigh channel results in poorer positioning performance.

Fig. 16 shows simulation results when the LOS probability [7] is applied to simulations for  $M \sim U[15, 25]$ , and the performance of the proposed technique and that of the conventional technique are compared for UEs at inner cell area (scenario-1:  $D^{(s)} = 100\text{m}$ ) and at outer cell area (scenario-2:  $D^{(s)} = 1\text{km}$ ). When a UE is close to the ENB<sub>s</sub>, LOS probability of the downlink of the ENB<sub>s</sub> is very high while that of the ENB<sub>n</sub> is very low for the UE at cell edge, so that the proposed technique outperforms the conventional technique in the scenario-1. However, when a UE is at the cell edge (scenario-2), the proposed technique does not provide noticeable performance improvement to the conventional technique as expected. In Fig. 16, the robust performance of the proposed technique is also demonstrated against some uncertainty in  $\sigma_c$ . In the simulations, we set 33% of uncertainty level in  $\sigma_c$ , however, the positioning performance does not show a noticeable performance degradation.

## VII. CONCLUSION

In this paper, we have derived the TOA error PDF of the resolved first arrival path of LTE PRS in GSMD-based statistical outdoor multipath environments such as urban and dense urban area, based on which the TDOA error PDF of the resolved first arrival path of LTE PRS has been derived for Rician and Rayleigh channels in outdoor urban environments. It has been demonstrated that the derived theoretical TDOA error distributions agree with the TDOA error histograms obtained from numerous Monte Carlo simulations based on GSMD. In addition, we have proposed an LTE TDOA positioning technique that compensates the expected TDOA

offset utilizing the statistical distribution of the mean TOA error. It is demonstrated that the proposed technique provides strong performance in urban environments when some of downlinks have Rayleigh channels and some downlink are in Rician channels.

## APPENDIX

Fig. 17 shows an ENB at  $B(D, 0)$  and a UE at  $O(0, 0)$  in a  $r\phi$ -polar coordinate system. The locations of scatterers causing multipath with the same excess delay  $\tau$  are on an ellipse whose foci are at the  $B$  and  $O$ . The area within the ellipse and the circular scattering region around the UE is segmented into multiple regions and shown for  $\phi \geq 0$ , where scatterer density around the UE follows the two-dimensional Gaussian distribution with variance  $\sigma^2$ , and  $R$  is a distance much larger than  $\sigma^2$ .

Let  $V_3$  be the probability mass over an area segment shown in Fig. 17 over  $\{r_0 \leq r \leq r_1, \max(\phi_0, \phi_1) \leq \phi \leq \pi\}$ , where  $\phi_0$  is the angle to the cross section point of the circle and the ellipse,  $\phi_1 = \pi/2$ , and  $r_0$  and  $r_1$  are the distance  $r$  for  $\phi = \pi$  and  $\phi = \phi_1$ , respectively. When TOA  $t$  is small,  $\phi_0$  is small, and, therefore, we assume that  $\phi_0 < \phi_1$  for TOAs with small delays. By inspection,  $V_3$  is negligibly small for  $0 \leq \phi_0 \leq \pi$ , and assuming  $\exp\{-r_0^2/2\sigma^2\} \approx \exp\{-r_1^2/2\sigma^2\} \simeq 1$  and  $tc \approx D$  for small  $\phi_0$  and large  $\sigma$ , the TOA error PDF for  $t > D/c$

$$\begin{aligned} f_t(t) &\simeq \frac{c}{\pi D} \left[ \exp\left(-\frac{r_1^2}{2\sigma^2}\right) - \exp\left(-\frac{r_0^2}{2\sigma^2}\right) \right] \\ &\quad + \frac{(\pi - 2)r_0 c}{4\pi\sigma^2} \exp\left(-\frac{r_0^2}{2\sigma^2}\right) + \frac{1}{\pi} \exp\left(-\frac{r_1^2}{2\sigma^2}\right) (\phi'_0 - Z_4) \\ &\quad + \frac{Z_5}{2\pi\sigma^2} \exp\left(-\frac{r_1^2}{2\sigma^2}\right) [r_0 Z_6 (Z_1 + Z_3) + Z_2 - RZ_3] \\ &\quad + \frac{2}{\sigma\sqrt{2\pi}} \left[ \frac{tc^2}{D} Q\left(\frac{r_0}{\sigma}\right) + (RZ_4 - \frac{tc^2}{D}) Q\left(\frac{r_1}{\sigma}\right) \right], \end{aligned} \quad (52)$$

where  $r_1 \simeq \frac{t^2 c^2 - D^2}{2tc}$ ,  $\phi'_0 \simeq \frac{tc^2}{RD} - \frac{c}{D}$ ,  $Z_1 = \frac{\pi}{2} - \phi_0 - \frac{tc}{D}$ ,  $Z_2 = \frac{r_0(D+tc)}{D}$ ,  $Z_3 = \frac{r_1(\pi/2-\phi_0)}{R-r_1}$ ,  $Z_4 = \frac{Rc[t^2 c^2 + D^2](\pi/2-\phi_0)}{2[Rtc-r_0(tc+D)]^2} - \frac{r_0(tc+\phi'_0)}{Rtc-r_0(tc+D)}$ ,  $Z_5 = \frac{c(t^2 c^2 + D^2)}{t^2 c^2}$ , and  $Z_6 = \frac{tc+D}{tc}$ .

## REFERENCES

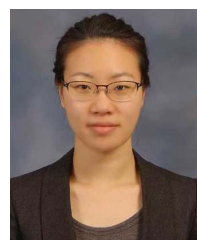
- [1] J. H. Reed, K. J. Krizman, B. D. Woerner, and T. S. Rappaport, "An overview of the challenges and progress in meeting the E-911 requirement for location service," *IEEE Commun. Mag.*, vol. 36, no. 4, pp. 30–37, Apr. 1998.
- [2] M. Moeglein and N. Krasner, *An Introduction to SnapTrack Server-Aided GPS Technology*. Beaumont, TX, USA: ION GPS, 1998.
- [3] 3GPP, "Universal terrestrial radio access (E-UTRA); stage 2 functional specification of user equipment (UE) positioning in EUTRAN (release 9)," TS36.305 V9.2.0, Mar. 2010.
- [4] TIA/EIA IS-801, "Position determination service standard for dual-mode spread spectrum systems," Oct. 1999.
- [5] M. Tayal, "Location services in the GSM and UMTS networks," in *Proc. IEEE ICPWC*, Jan. 2005, pp. 373–378.
- [6] R. M. Vaghefi and R. M. Buehrer, "Improving positioning in LTE through collaboration," in *Proc. 11th Workshop Positioning, Navigat. Commun. (WPNC)*, Dresden, Germany, Mar. 2014, pp. 1–6.
- [7] 3GPP, "Technical specification group radio access network: Study on 3D channel model for LTE," TR36.873 V12.0.0, Sep. 2014.

- [8] S.-H. Kong, "TOA and AOD statistics for down link Gaussian scatterer distribution model," *IEEE Trans. Wireless Commun.*, vol. 8, no. 5, pp. 2609–2617, May 2009.
- [9] S.-H. Kong, "Analysis of code phase estimation error from resolved first arrival path," *IEEE Trans. Aerosp. Electron. Syst.*, vol. 50, no. 4, pp. 2456–2467, Oct. 2014.
- [10] E. Steingass and A. L. German, "Measuring the navigation multipath channel—A statistical analysis," in *Proc. 17th Int. Tech. Meeting Satellite Division Inst. Navigat. (ION GNSS)*, Long Beach, CA, USA, Sep. 2004, pp. 1157–1164.
- [11] P. Misra and P. Enge, *Global Positioning System: Signals, Measurements, and Performance*, 2nd ed. Lincoln, MA, USA: Ganga-Jamuna Press, 2006.
- [12] W. Xu, M. Huang, C. Zhu, and A. Dammann, "Maximum likelihood TOA and OTDOA estimation with first arriving path detection for 3GPP LTE system," *Trans. Emerg. Telecommun. Technol.*, vol. 27, pp. 339–356, Mar. 2016.
- [13] W. Nam and S.-H. Kong, "Least-squares-based iterative multipath super-resolution technique," *IEEE Trans. Signal Process.*, vol. 61, no. 3, pp. 519–529, Feb. 2013.
- [14] O. Bialer, D. Raphaeli, and A. J. Weiss, "Efficient time of arrival estimation algorithm achieving maximum likelihood performance in dense multipath," *IEEE Trans. Signal Process.*, vol. 60, no. 3, pp. 1241–1252, Mar. 2012.
- [15] J. A. del Peral-Rosado, J. A. López-Salcedo, G. Seco-Granados, F. Zanier, and M. Crisci, "Joint maximum likelihood time-delay estimation for LTE positioning in multipath channels," *EURASIP J. Adv. Signal Process.*, vol. 2014, no. 33, pp. 1–13, Feb. 2014.
- [16] T. Wang, Y. Shen, S. Mazuelas, H. Shin, and M. Z. Win, "On OFDM ranging accuracy in multipath channels," *IEEE Syst. J.*, vol. 8, no. 1, pp. 104–114, Mar. 2014.
- [17] "Evolved universal terrestrial radio access (E-TURA); base station (BS) radio transmission and reception," 3GPP, Tech. Rep. TS 36.104 V9.13.0, Sep. 2012.
- [18] P. Kyösti, J. Meinilä, L. Hentila, and T. Rautiainen, "WINNER II channel models," IST-WINNER D1.1.2 V1.2, 2007.
- [19] J. Medbo, I. Siomina, A. Kangas, and J. Furuskog, "Propagation channel impact on LTE positioning accuracy: A study based on real measurements of observed time difference of arrival," in *Proc. Pers. Indoor Mobile Radio Commun. (PIMRC)*, 2009, pp. 2213–2217.
- [20] J. A. del Peral-Rosado, J. A. López-Salcedo, G. Seco-Granados, F. Zanier, and M. Crisci, "Evaluation of the LTE positioning capabilities under typical multipath channels," in *Proc. 6th IEEE Adv. Satellite Multimedia Syst. Conf. (ASMS)*, Sep. 2012, pp. 139–146.
- [21] C. Gentner, E. Muñoz, M. Khider, E. Staudinger, S. Sand, and A. Dammann, "Particle filter based positioning with 3GPP-LTE in indoor environments," in *Proc. IEEE/ION Position Location Navigat. Symp. (PLANS)*, Myrtle Beach, SC, USA, Apr. 2012, pp. 301–308.
- [22] W. Wang, T. Jost, C. Mensing, and A. Dammann, "ToA and TDOfA error models for NLoS propagation based on outdoor to indoor channel measurement," in *Proc. IEEE Wireless Commun. Netw. Conf. (WCNC)*, Budapest, Hungary, Apr. 2009, pp. 1–6.
- [23] D. Bladsjö, M. Hogan, and S. Ruffini, "Synchronization aspects in LTE small cells," *IEEE Commun. Mag.*, vol. 51, no. 9, pp. 70–77, Sep. 2013.
- [24] R. Janaswamy, "Angle and time of arrival statistics for the Gaussian scatter density model," *IEEE Trans. Wireless Commun.*, vol. 1, no. 3, pp. 488–497, Jul. 2002.
- [25] M. P. Löter and P. Van Rooyen, "Modeling spatial aspects of cellular CDMA/SDMA systems," *IEEE Commun. Lett.*, vol. 3, no. 5, pp. 128–131, May 1999.
- [26] J. A. del Peral-Rosado, "Evaluation of the LTE positioning capabilities in realistic navigation channels," Ph.D. dissertation, Univ. Autònoma de Barcelona (UAB), Barcelona, Spain, Mar. 2014.
- [27] J. A. Del Peral-Rosado, J. A. López-Salcedo, G. Seco-Granados, F. Zanier, and M. Crisci, "Achievable localization accuracy of the positioning reference signal of 3GPP LTE," in *Proc. IEEE Int. Conf. Localization GNSS (ICL-GNSS)*, Jun. 2012, pp. 1–6.
- [28] A. Papoulis, *Probability, Random Variables and Stochastic Processes*, 3rd ed. New York, NY, USA: McGraw-Hill, 1991.
- [29] G. K. Karagiannidis and A. S. Lioumpas, "An improved approximation for the Gaussian Q-function," *IEEE Commun. Lett.*, vol. 11, no. 8, pp. 644–646, Aug. 2007.
- [30] I. Jami and R. Ormondroyd, "Estimation of the scattering radius around a mobile handset using a sub-space technique," in *Proc. IEEE EUROCOMM Inf. Syst. Enhanced Public Safety Secur.*, May 2000, pp. 131–135.
- [31] N. Chen, M. Tanaka, and R. Heaton, "OFDM timing synchronisation under multi-path channels," in *Proc. IEEE 57th Veh. Technol. Conf. (VTC)*, vol. 1. Jeju, South Korea, Apr. 2003, pp. 378–382.
- [32] W. C. Jakes, Ed., *Microwave Mobile Communications*. Piscataway, NJ, USA: IEEE Press, 1974.
- [33] A. Goldsmith, *Wireless Communications*. Cambridge, U.K.: Cambridge Univ. Press, 2005.
- [34] S.-H. Kong, "Statistical analysis of urban GPS multipaths and pseudo-range measurement errors," *IEEE Trans. Aerosp. Electron. Syst.*, vol. 47, no. 2, pp. 1101–1113, Apr. 2011.
- [35] A. A. M. Saleh and R. A. Valenzuela, "A statistical model for indoor multipath propagation," *IEEE J. Sel. Areas Commun.*, vol. SAC-5, no. 2, pp. 128–137, Feb. 1987.
- [36] W.-J. Chang and J.-H. Tarn, "Effects of bandwidth on observable multipath clustering in outdoor/indoor environments for broadband and ultrawideband wireless systems," *IEEE Trans. Veh. Technol.*, vol. 56, no. 4, pp. 1913–1923, Jul. 2007.
- [37] H. A. David and H. N. Nagaraja, *Order Statistics*. New York, NY, USA: Wiley, 1970.
- [38] N. Dyson, *Chromatographic Integration Methods*, 2nd ed. London, U.K.: Royal Society of Chemistry, 1998.
- [39] 3GPP TR 36.942 V9.3.0, "Evolved universal terrestrial radio access (E-UTRA); radio frequency (RF) system scenarios," Jul. 2012.
- [40] S. M. Kay, *Fundamentals of Statistical Signal Processing: Estimation Theory*. Upper Saddle River, NJ, USA: Prentice-Hall, 1998.
- [41] S. Bartoletti, W. Dai, A. Conti, and M. Z. Win, "A mathematical model for wideband ranging," *IEEE J. Sel. Topics Signal Process.*, vol. 9, no. 2, pp. 216–228, Mar. 2015.
- [42] D. Muñoz, F. B. Lara, C. Vargas, and R. Enríquez-Calderá, *Position Location Techniques and Applications*. San Diego, CA, USA: Academic, 2009.
- [43] 3GPP TR 36.331 V12.0.0, "Evolved universal terrestrial radio access (E-UTRA); radio resource control (RRC); protocol specification," Jan. 2014.
- [44] 3GPP TR36.873 V13.1.0, "Study on indoor positioning enhancements for UTRA and LTE," Dec. 2015.
- [45] Y. Karasawa, "Statistical multipath propagation modeling for broadband wireless systems," *IEICE Trans. Commun.*, vol. E90-B, no. 3, pp. 468–484, Mar. 2007.



**Seung-Hyun Kong** (M'06–SM'16) received the B.S. degree in electronics engineering from Sogang University, South Korea, in 1992, the M.S. degree in electrical engineering from Polytechnic University, New York, NY, USA, in 1994, and the Ph.D. degree in aeronautics and astronautics from Stanford University, Stanford, CA, USA, in 2006. From 1997 to 2004, he was with Samsung Electronics Inc., South Korea and Nexpilot Inc., South Korea, where his research focus was on wireless communication systems and UMTS mobile positioning technologies.

From 2007 to 2009, he was a Staff Engineer with Polaris Wireless Inc., Santa Clara, CA, USA, and with the Corporate R&D of Qualcomm Inc., San Diego, CA, USA, where his research was on assisted-GNSS, wireless location signature, and mobile-to-mobile positioning technologies. Since 2010, he has been with the Korea Advanced Institute of Science and Technology (KAIST), where he is currently an Associate Professor with the CCS Graduate School for Green Transportation. His research interests include next generation GNSS, advanced signal processing for navigation systems, and vehicular communication systems.



**Binhee Kim** (M'15) received the B.S. and M.S. degrees in electrical engineering from the Korea Advanced Institute of Science and Technology (KAIST), Daejeon, South Korea, in 2008 and 2010, respectively, and the Ph.D. degree from KAIST in 2015. She is a Researcher with the CCS Graduate School for Green Transportation, KAIST. Her research interests include radar signal processing, GNSS signal processing, and detection and estimation for navigation systems.